

# Numerical Simulation of Pressure Waves in the Cochlea Induced by a Microwave Pulse

Nir M. Yitzhak, Raphael Ruppin,\* and Ronen Hareuveny

*Radiation Safety Division, Soreq Nuclear Research Center, Yavne, Israel*

The pressure waves developing at the cochlea by the irradiation of the body with a plane wave microwave pulse are obtained by numerical simulation, employing a two-step finite-difference time-domain (FDTD) algorithm. First, the specific absorption rate (SAR) distribution is obtained by solving the Maxwell equations on a FDTD grid. Second, the temperature rise due to this SAR distribution is used to formulate the thermoelastic equations of motion, which are discretized and solved by the FDTD method. The calculations are performed for anatomically based full body human models, as well as for a head model. The dependence of the pressure amplitude at the cochlea on the frequency, the direction of propagation, and the polarization of the incident electromagnetic radiation, as well as on the pulse width, was investigated. *Bioelectromagnetics* 35:491–496, 2014.

© 2014 Wiley Periodicals, Inc.

**Key words:** thermoelastic; FDTD; auditory effect; finite-difference time-domain

## INTRODUCTION

Pulsed microwave radiation can produce a hearing sensation in human beings, which manifests itself as a clicking, buzzing, or hissing sound. The first systematic experimental studies of this effect were performed by Frey [1961, 1962], and the correct identification of the thermoelastic expansion as the mechanism responsible for the effect has been proposed by Foster and Finch [1974]. The absorption of the microwave energy produces a rapid thermal expansion, resulting from a small temperature rise of  $10^{-6}$  °C. This launches a thermoelastic wave of acoustic pressure that travels to the cochlea. An early detailed review of the auditory effect has been presented by Lin [1978], and more recently, the subject has been reviewed by Elder and Chou [2003] and by Lin and Wang [2007].

The first analytic models for calculating the sound pressure amplitude inside the head due to a microwave pulse using a homogeneous spherical model of the head, and assuming a specific spherically symmetric heating pattern peaked at the sphere center were developed by Lin [1977a, b]. Shibata et al. [1986] employed Lin's method, but with an improved specific heating pattern. A generalization of the analytic method, again using a homogeneous sphere head model, but with an arbitrary microwave absorption pattern of spherical symmetry, has been presented by Yitzhak et al. [2009]. The work of Watanabe et al. [2000] is the first in which anatomically based head models were used to calculate the pressure waves generated by the thermoelastic expansion. This finite-

difference time-domain (FDTD) calculation was performed at only one frequency, 915 MHz, with plane wave irradiation. Lin and Wang [2010] used the FDTD method to calculate the pressure generated in an anatomic head model placed inside a birdcage MRI coil, driven by a rectangular current pulse. The use of a head model for calculating the effects of external electromagnetic fields, rather than using a whole body model, is justified when the fields arise from a localized source located near the head. This is the case for birdcage magnetic resonance imaging (MRI) coils [Lin and Wang, 2010] and also for mobile phones, for which many specific absorption rate (SAR) calculations have been performed using detailed anatomical head (or head and shoulders) models [Martinez-Burdalo et al., 2004; Keshvari and Lang, 2005; Christ et al., 2010; Lu and Ueno, 2012]. However, when the electromagnetic source is not too close to the irradiated body, so that the incident fields can be represented by plane waves, a whole body model has to be used in order to correctly analyze the problem. In the context of the microwave hearing effect, this has not been implemented before. Here we employ full body

\*Correspondence to: Raphael Ruppin, Radiation Safety Division, Soreq Nuclear Research Center Yavne 81800, Israel. E-mail: ruppin@soreq.gov.il

Received for review 18 December 2013; Accepted 25 May 2014

DOI: 10.1002/bem.21869

Published online 6 August 2014 in Wiley Online Library (wileyonlinelibrary.com).

models for FDTD calculations of the SAR and the subsequent excitation of pressure waves by the thermoelastic effect. For comparison, some computations for a head model will also be presented. This study covers a wide electromagnetic frequency range, between 40 MHz and 3 GHz.

## FDTD METHOD OF CALCULATION

### SAR Calculation

The interaction of an incident electromagnetic plane wave with three different biological models was calculated numerically using the Yee FDTD algorithm [Yee, 1966] for solving Maxwell's curl equations. For this step, the commercial software XFDTD (Remcom, State College, PA) was employed. The following models, also supplied by Remcom, were used: (1) Male body, with the height of 1.875 m, resolution of  $5 \times 5 \times 5 \text{ mm}^3$  and 39 different tissue types; (2) Female body, with the height of 1.725 m, resolution of  $5 \times 5 \times 5 \text{ mm}^3$  and 32 different tissue types; (3) Male head and shoulders, with the height of 0.348 m, resolution of  $2 \times 2 \times 2 \text{ mm}^3$  and 26 different tissue types. The meshes of these models were converted directly from the data generated by the Visible Human Project sponsored by the U.S. National Library of Medicine. Using the calculated SAR distribution, the temperature rise  $\theta(x, y, z, t)$  caused by a rectangular pulse of width  $\tau$  is given by  $\theta = \text{SAR} \cdot t / C_h$  for  $0 \leq t \leq \tau$  and by  $\theta = \text{SAR} \cdot \tau / C_h$  for  $t > \tau$ , where  $C_h$  is the tissue specific heat. The temperature decay processes can be neglected, because they are slow in comparison with the time durations considered herein, 1 ms.

### Thermoelastic Equations

The thermoelastic equations of motion are given by [Landau and Lifshitz, 1986]

$$\frac{\partial \sigma_{ij}}{\partial t} = \mu \left( \frac{\partial v_i}{\partial x_j} + \frac{\partial v_j}{\partial x_i} \right) + \lambda \delta_{ij} \frac{\partial v_k}{\partial x_k} - (3\lambda + 2\mu) \alpha \delta_{ij} \frac{\partial \theta}{\partial t} \quad (1)$$

where the Einstein summation convention is used. Here,  $\sigma_{ij}$  are the rectangular components of the stress tensor,  $v_i$  are the components of the particle velocity,  $\lambda$  and  $\mu$  are the Lamé elastic coefficients and  $\alpha$  is the coefficient of linear thermal expansion. The six equations represented by (1) have to be solved together with the three Newton equations

$$\rho \frac{\partial v_i}{\partial t} = \frac{\partial \sigma_{ij}}{\partial x_j} \quad (2)$$

where  $\rho$  is the tissue mass density. The systems of Equations (1) and (2) are discretized and solved numerically using the FDTD method. A Yee type explicit leapfrog time stepping scheme is employed, in which the stress tensor components and the velocity components are alternately updated [Watanabe et al., 2000]. The pressure is obtained from the stress tensor by  $p = \sigma_{ii}/3$ . Since a rectangular pulse contains high frequency components that cannot be handled by the FDTD method, we used a slightly rounded pulse, with

$$\frac{\partial \theta}{\partial t} = \frac{\text{SAR}}{2C_h} [\text{erf}(at) - \text{erf}(a(t - \tau))] \quad (3)$$

where the value  $a = 4 \times 10^5 \text{ s}^{-1}$  is chosen for the pulse steepness parameter [Watanabe et al., 2000]. Whenever the boundary of the biological model is surrounded by air, the stress free boundary condition is used. This is not appropriate for the bottom layer of the head model, so in this case, an absorbing perfectly matched layer (PML; with a 10 cell thickness) was added [Chew and Liu, 1996]. We verified the accuracy of the elastic FDTD algorithm by applying it to the homogeneous sphere case, for which analytic solutions are available for comparison [Yitzhak et al., 2009].

### Choice of Physical Parameters

The electromagnetic parameters, that is, the frequency dependent conductivities and permittivities of the tissues, were supplied by Remcom with the biological models, as were the densities and the specific heats, which are needed for the temperature rise calculation. For the Lamé elastic parameters of the soft tissues, the values  $\lambda = 2.1 \text{ GPa}$  and  $\mu = 22.3 \text{ kPa}$  will be employed [Margulies and Meaney, 1998]. For the bone tissues, the values  $\lambda = 6.9 \text{ GPa}$  and  $\mu = 4.6 \text{ GPa}$  have been employed in previous FDTD calculations [Watanabe et al., 2000; Lin and Wang, 2010]. However, this choice (based on data of Goel et al. [1994]), with  $\lambda > \mu$ , does not seem to be representative, since it is usually found that for bone tissues  $\mu > \lambda$  [Chu et al., 1994; Zhang et al., 2001; Gong et al., 2008]: We will employ the values  $\lambda = 1.8 \text{ GPa}$  and  $\mu = 2.7 \text{ GPa}$  [Chu et al., 1994]. For the coefficient of linear thermal expansion, the values  $\alpha = 13 \times 10^{-5}/^\circ\text{C}$  for soft tissues,  $\alpha = 2.7 \times 10^{-5}/^\circ\text{C}$  for bone tissues, and  $\alpha = 31 \times 10^{-5}/^\circ\text{C}$  for fat will be used [Duck, 1990]. In his analytic calculations, and in the absence of experimental data, Lin [1977a, b] used a value equal to 60% of the corresponding value for water, that is,  $\alpha = 4.1 \times 10^{-5}/^\circ\text{C}$  for the coefficient of thermal expansion of soft tissues. In subsequent FDTD

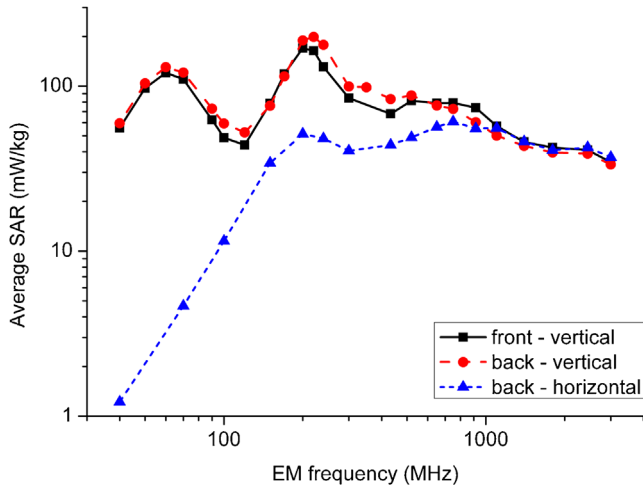


Fig. 1. Electromagnetic frequency dependence of the average SAR in the head as calculated for the male body model.

calculations of the microwave auditory effect [Watanabe et al., 2000; Lin and Wang, 2010], this value was again employed. However, experimental data [Duck, 1990] indicate that the thermal expansion coefficient of soft tissues is in fact higher than that of water. Since the thermal expansion coefficient appears in Equation (1) in the source term of the thermoelastic effect, the pressure levels calculated here with an experimentally based parameter choice will be higher than those obtained previously for the head model [Watanabe et al., 2000].

**RESULTS**

**SAR Calculations**

For all three models, we define the head region (for the purpose of calculating the average SAR of the head) as that volume of the model, which is terminated by a horizontal plane just below the chin. This head region has a mass of 5.871 kg for the female body model, 6.578 kg for the male body model and 6.390 kg for the male head and shoulders model. The frequency dependence of the average SAR in the head, as calculated for the male model, is shown in Figure 1. Here, as well as in all other calculations presented in this paper, an incident power density of 1 mW/cm<sup>2</sup> is assumed. The electromagnetic plane wave radiation is incident from either the front side or the backside, and its polarization is either vertical or horizontal. For the vertical polarization there occurs a peak at about 60 MHz, which corresponds to the well known whole body resonance [Dimbylow, 1997, 2002]. For both polarizations there occurs a peak at around 200 MHz, and another broader one around 750 MHz. A compari-

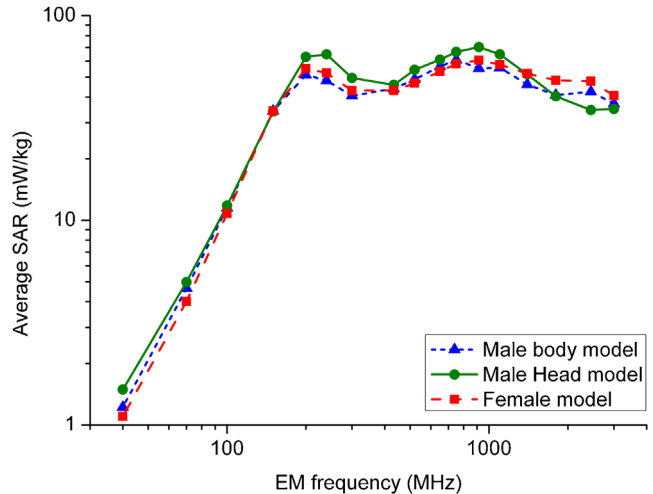


Fig. 2. Electromagnetic frequency dependence of the average SAR in the head as calculated for the three models, assuming incidence from the backside, with horizontal polarization.

son of the head average SAR of the three models (male, female and head and shoulders) for horizontally polarized irradiation from the back is shown in Figure 2. It is found that for this polarization, the SAR frequency dependence is similar in the different models.

**Pressure Waves and Power Spectra**

Typical examples of the pressure waves which develop in the cochlea in the three models are shown in Figure 3. These were calculated for a plane wave pulse of frequency 915 MHz incident from the back side, with horizontal polarization, pulse width of 70 μs. Figure 4 shows the corresponding power

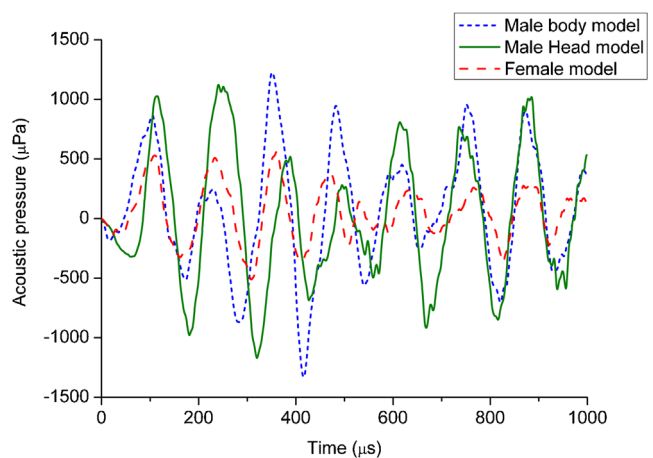


Fig. 3. Calculated pressure waveform at the cochlea for the three models, for irradiation from the backside by a horizontally polarized 915 MHz pulse of 70 μs width.

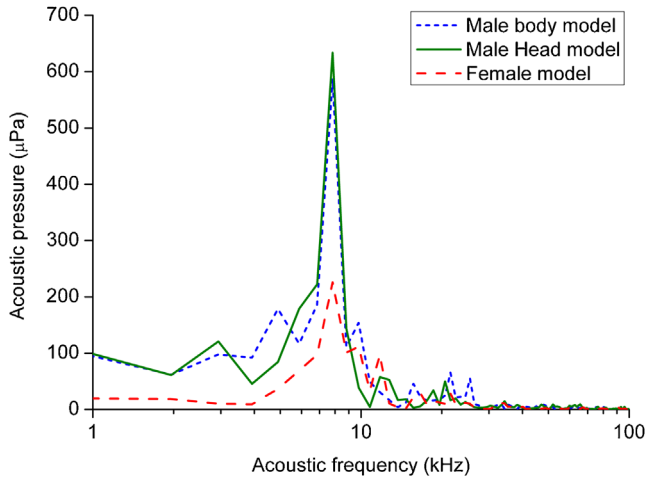


Fig. 4. Calculated power spectra of the pressure waves at the cochlea for the three models, for irradiation from the backside by a horizontally polarized 915 MHz pulse of 70 μs width.

spectra, obtained by performing a Fast Fourier Transform (FFT) on the time dependent waves. The FFT was performed over 1.02 ms after the end of the pulse. In all models, the strongest acoustic response occurs at the frequency of about 8 kHz, which represents the fundamental resonance frequency of sound generation in the human head [Lin, 1977a,b; Watanabe et al., 2000; Lin and Wang, 2010]. The occurrence of a peak in the acoustic power spectrum near 8 kHz persists also for other electromagnetic frequencies, irradiation directions, polarizations and pulse widths, although secondary peaks, in the range between 1 kHz and about 30 kHz also appear. We checked the effect of the finite integration time on the power spectrum, by performing an extended time calculation for one specific case. It was found that the short integration time result has a similar spectral content, but with a wider main peak.

**Pulse Width Dependence of Pressure Amplitudes**

In the case of the homogeneous spherical head model, for which analytical solutions have been derived [Lin, 1977a,b; Yitzhak et al., 2009] it was found that the pulse width dependence of the induced pressure amplitude at a given location in the head, and at an acoustic angular frequency ω<sub>m</sub> is of the form

$$P(\tau) = A \left| \sin\left(\frac{\omega_m \tau}{2}\right) \right| \tag{4}$$

here, τ is the pulse width and the amplitude factor A is independent of the pulse width. We have found that this dependence on the pulse width holds to a good

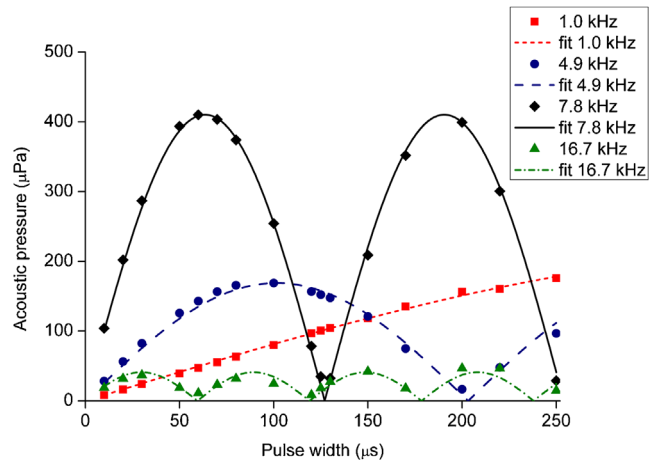


Fig. 5. Pulse width dependence of the amplitude of a number of acoustic frequencies. The curves were obtained by fitting to the form of Equation (4), calculated for the male body model irradiated from the front by a vertically polarized 915 MHz pulse.

approximation even for the complicated biological models treated here. This is exemplified by Figure 5, in which the pulse width dependence of the amplitudes of a number of selected acoustic frequencies, as obtained by a Fourier decomposition of the pressure in the cochlea, is shown by the discrete points. The corresponding curves were obtained by fitting the calculated points to the functional form of Equation (4), using a nonlinear least squares algorithm.

The pulse width dependence of the pressure amplitude (RMS value) at the cochlea, due to a 915 MHz pulse, for different irradiation directions and polarizations, is shown in Figure 6. In comparing to

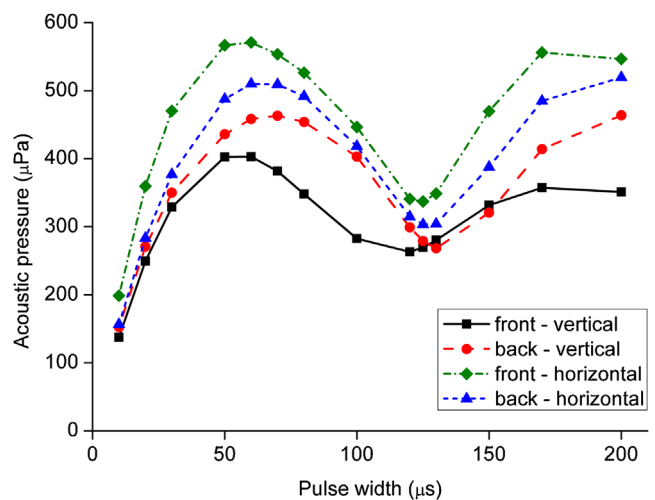


Fig. 6. Calculated pulse width dependence of the pressure amplitude at the cochlea for the male model irradiated by a 915 MHz pulse, for different incidence directions and polarizations.

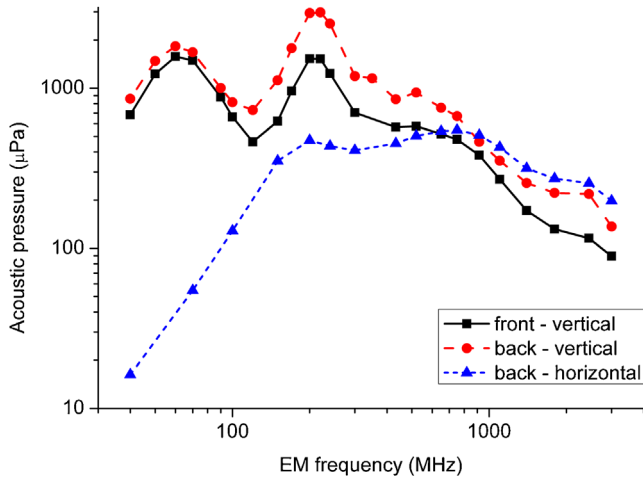


Fig. 7. Calculated frequency dependence of the pressure amplitude at the cochlea for the male model irradiated by a pulse of a width of 70  $\mu$ s.

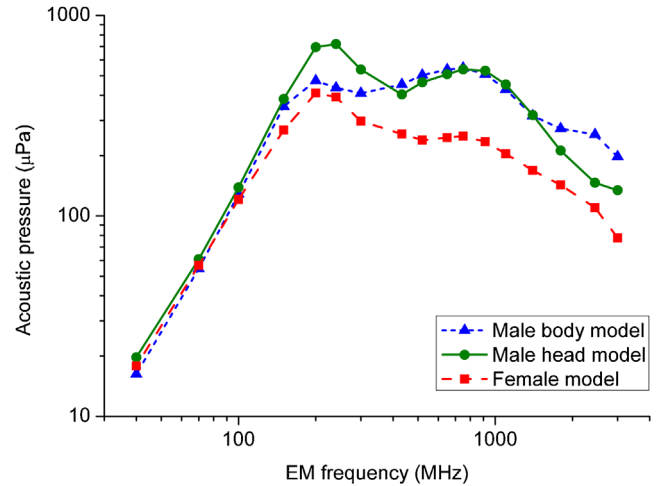


Fig. 8. Calculated frequency dependence of the pressure amplitude at the cochlea for the three models for irradiation from the backside with a horizontally polarized pulse of 70  $\mu$ s width.

Figure 5, this dependence reflects the dominance of the 8 kHz region in the acoustic response (Fig. 4). Previous calculations on a head model [Watanabe et al., 2000] as well as experimental data [Tyazhelov et al., 1979] displayed similar characteristics.

**Electromagnetic Frequency Dependence of Pressure Amplitudes**

We have investigated the electromagnetic frequency dependence of the RMS acoustic pressure developing in the cochlea. The results for the male body model are shown in Figure 7. For the vertical polarization, there appear two distinct maxima at around 60 MHz and close to 200 MHz. In the horizontal polarization case, the low frequency peak disappears completely. These features clearly reflect the frequency dependence of the average SAR in the head, as shown in Figure 1. A comparison of the frequency dependence of the pressure at the cochlea in the three biological models is shown in Figure 8. Again, the general features of these spectra exhibit a correlation with the corresponding average head SAR spectra of Figure 2, but to a lesser degree for the woman model at the higher frequencies. The calculations of Figures 7 and 8 refer to a pulse width of 70  $\mu$ s, but we have found that the dependence on the electromagnetic frequency is similar for pulse widths in the range of 10–250  $\mu$ s.

The pressure threshold value for bone conduction hearing (which is the mechanism responsible for the microwave auditory effect) is estimated at about 58 dB (Re 20  $\mu$ Pa) for acoustic frequencies around 8 kHz

[Zwislocki, 1957]. However, this value was measured with a pulse width of 200 ms. The corresponding thresholds for shorter pulses will be estimated using the experimental data of Thurlow and Bowman [1957]. They found that a 10-fold decrease in pulse duration yields an 8 dB increase in threshold. We will estimate the electromagnetic power density threshold for the auditory effect for incident pulses of 2450 MHz, widths of 10 and 20  $\mu$ s, and pulse repetition rate of 3 s<sup>-1</sup>, as in the experiments of Guy et al. [1975]. Using the data of Zwislocki [1957] and correcting for the pulse width and pulse repetition rate, using the data of Thurlow and Bowman [1957], we find that the pressure threshold values for bone conduction hearing are 940 and 715 mPa for 10 and 20  $\mu$ s pulses, respectively. Our FDTD calculations for the male model irradiated from the backside at 2450 MHz (vertical polarization) yielded pressures of 88.7 and 144  $\mu$ Pa, for pulse widths of 10 and 20  $\mu$ s, respectively. Since these values were obtained with an incident power density of 1 mW/cm<sup>2</sup>, the power density required to induce the auditory effect is about 10600 mW/cm<sup>2</sup> for the 10  $\mu$ s pulse width and about 4960 mW/cm<sup>2</sup> for the 20  $\mu$ s pulse width. The corresponding threshold levels for the auditory response measured by Guy et al. [1975] were 4000 and 2150 mW/cm<sup>2</sup>, respectively.

**CONCLUSION**

Full body biological models were used to calculate the excitation of pressure waves at the cochlea,

following the irradiation by a microwave pulse. The dependence of the amplitude of the pressure waves on the microwave frequency was found to exhibit a correlation with the average SAR in the head. This SAR displays a number of peaks, one of them occurring (for vertically polarized incident radiation) at the full body resonance ( $\sim 60$  MHz for the male model). Thus, for plane wave excitation, calculations based on head models (rather than full body models) cannot fully predict the correct electromagnetic frequency dependence of the auditory effect. On the other hand, the dependence of the pressure wave amplitude on the pulse width obtained with full body models is similar to that derived with head models.

We have shown, by a Fourier decomposition of the pressure waves in the cochlea, that the pulse width dependence of the amplitudes at various acoustic frequencies obeys the simple sinusoidal relation (Equation 4). This is due to the fact that for the complicated biological model, there exists an effective resonant cavity for each acoustic frequency. However, the power spectra of the pressure waves at the cochlea are dominated by the acoustic head resonance at about 8 kHz.

## REFERENCES

- Chew WC, Liu QH. 1996. Perfectly matched layers for elastodynamics: A new absorbing boundary condition. *J Comput Acoust* 4:341–359.
- Christ A, Gosselin MC, Christopoulou M, Kühn S, Kuster N. 2010. Age-dependent tissue-specific exposure of cell phone users. *Phys Med Biol* 55:1767–1783.
- Chu CS, Lin MS, Huang HM, Lee MC. 1994. Finite element analysis of cerebral contusion. *J Biomech* 27:187–194.
- Dimbylow PJ. 1997. FDTD calculations of the whole body averaged SAR in an anatomically realistic voxel model of the human body from 1 MHz to 1 GHz. *Phys Med Biol* 42:479–490.
- Dimbylow PJ. 2002. Fine resolution calculations of SAR in the human body for frequencies up to 3 GHz. *Phys Med Biol* 47:2835–2846.
- Duck FA. 1990. Physical properties of tissue: A comprehensive reference book. London: Academic Press. pp 137–165.
- Elder JA, Chou CK. 2003. Auditory response to pulsed radio-frequency energy. *Bioelectromagnetics* 24:S162–S173.
- Foster KR, Finch ED. 1974. Microwave hearing: Evidence for thermoacoustic auditory stimulation by pulsed microwaves. *Science* 185:256–258.
- Frey AH. 1961. Auditory system response to radio frequency energy. *Aerosp Med* 32:1140–1142.
- Frey AH. 1962. Human auditory system response to modulated electromagnetic energy. *J Appl Physiol* 17:689–692.
- Goel VK, Park H, Kong W. 1994. Investigation of vibration characteristics of the ligamentous lumbar spine using the finite element approach. *J Biomech Eng* 116:337–383.
- Gong SW, Lee HP, Lu C. 2008. Dynamic response of a human head to a foreign object impact. *IEEE Trans Biomedical Eng* 55:1226–1229.
- Guy AW, Chou CK, Lin JC, Christensen D. 1975. Microwave induced acoustic effects in mammalian auditory systems and physical materials. *Ann N Y Acad Sci* 247:194–215.
- Keshvari J, Lang S. 2005. Comparison of radio frequency energy absorption in ear and eye region of children and adults at 900, 1800 and 2450 MHz. *Phys Med Biol* 50:4355–4369.
- Landau LD, Lifshitz EM. 1986. Theory of Elasticity. Oxford: Pergamon Press.
- Lin JC. 1977a. On microwave induced hearing sensation. *IEEE Trans Microw Theory Tech* 25:605–613.
- Lin JC. 1977b. Further studies on the microwave auditory effect. *IEEE Trans Microw Theory Tech* 25:938–943.
- Lin JC. 1978. Microwave Auditory Effects and Applications. Springfield, IL: Charles C. Thomas.
- Lin JC, Wang Z. 2007. Hearing of microwave pulses by humans and animals: Effects, mechanism, and thresholds. *Health Phys* 92:621–628.
- Lin JC, Wang Z. 2010. Acoustic pressure waves induced in human heads by RF pulses from high-field MRI scanners. *Health Phys* 98:603–613.
- Lu M, Ueno S. 2012. Comparison of specific absorption rate induced in brain tissues of a child and an adult using mobile phone. *J Appl Phys* 111:07B311–07B313.
- Margulies SS, Meaney DF. 1998. Brain tissues. In: Handbook of biomaterial properties. Black J and Hastings G, editors. London: Chapman and Hall. pp 70–80.
- Martinez-Burdalo M, Martin A, Anguiano M, Villar R. 2004. Comparison of FDTD-calculated specific absorption rate in adults and children when using a mobile phone at 900 and 1800 MHz. *Phys Med Biol* 49:345–354.
- Shibata T, Fujiwara O, Katoh K, Azakami T. 1986. Calculation of thermal stress inside human head by pulsed microwave irradiation. *IEICE Trans Commun* J69-B:1144–1146.
- Thurlock WR, Bowman R. 1957. Threshold for thermal noise as a function of duration and interruption rate. *J Acoust Soc Am* 29:281–283.
- Tyazhelov VV, Tigranian RE, Khizhniak EO, Akoef IG. 1979. Some peculiarities of auditory sensations evoked by pulsed microwave fields. *Radio Sci* 14:259–263.
- Watanabe Y, Tanaka T, Taki M, Watanabe S. 2000. FDTD analysis of microwave hearing effect. *IEEE Trans Microw Theory Tech* 48:2126–2132.
- Yee KS. 1966. Numerical solution of initial boundary value problems involving Maxwell's equations in isotropic media. *IEEE Trans Antenna Propag* 14:302–307.
- Yitzhak NM, Ruppin R, Hareuveny R. 2009. Generalized model of the microwave auditory effect. *Phys Med Biol* 54:4037–4049.
- Zhang L, Yang KH, King AI. 2001. Comparison of brain response between frontal and lateral impacts by finite element modeling. *J Neurotrauma* 18:21–30.
- Zwislocki J. 1957. In search of the bone-conduction threshold in a free sound field. *J Acoust Soc Am* 29:795–804.